

See discussions, stats, and author profiles for this publication at: <https://www.researchgate.net/publication/281146163>

# Optically Bistable Macroporous Photonic Crystals Enabled by Thermoresponsive Shape Memory Polymers

ARTICLE *in* ADVANCED OPTICAL MATERIALS · AUGUST 2015

Impact Factor: 4.06 · DOI: 10.1002/adom.201500277

---

READS

40

## 9 AUTHORS, INCLUDING:



[Yongliang Ni](#)

University of Florida

6 PUBLICATIONS 1 CITATION

[SEE PROFILE](#)



[Bingchen Wang](#)

University of Florida

2 PUBLICATIONS 0 CITATIONS

[SEE PROFILE](#)



[Vito Basile](#)

Italian National Research Council

9 PUBLICATIONS 1 CITATION

[SEE PROFILE](#)



[Curtis R. Taylor](#)

University of Florida

46 PUBLICATIONS 241 CITATIONS

[SEE PROFILE](#)

# Optically Bistable Macroporous Photonic Crystals Enabled by Thermoresponsive Shape Memory Polymers

Yin Fang, Sin-Yen Leo, Yongliang Ni, Long Yu, Pengxu Qi, Bingchen Wang,  
Vito Basile, Curtis Taylor, and Peng Jiang\*

Photonic crystals are periodic dielectric structures with a forbidden band gap for electromagnetic waves, analogous to the electronic band gap in semiconductors.<sup>[1–4]</sup> Photons with energies lying in this photonic band gap (PBG) cannot propagate through the dielectric medium, providing vast opportunities in controlling the flow of light in miniature volumes for a large variety of applications ranging from all-optical integrated circuits to quantum information processing.<sup>[1,5]</sup> Compared with conventional photonic crystals with fixed PBGs which are useful for developing passive nanooptical devices, tunable photonic crystals with adjustable PBGs have recently attracted great research interest as they could enable active devices, like low-threshold tunable lasers, full-color displays, optical switches, and chemical sensors.<sup>[6–17]</sup> A large variety of tuning mechanisms, such as mechanical pressure, temperature variation, electrical and magnetic fields, solvent swelling, and redox reactions, have been exploited to change either the photonic crystal structural parameters (e.g., lattice constant and crystalline structure) or the effective refractive index of the diffractive media.<sup>[10,18–28]</sup> For instance, mechanical pressure is a commonly used driving force for tuning the crystalline lattice spacing of soft photonic crystals consisting of elastic materials (e.g., elastomers and gels).<sup>[18,19,26]</sup> Externally applied magnetic fields have been extensively explored in controlling the

assembled structures of magnetic nanoparticles to achieve tunable PBGs.<sup>[25,29,30]</sup> Refractive index tuning is also widely utilized in altering structural colors.<sup>[17,27,31]</sup> However, traditional tunable photonic crystals usually cannot memorize the temporarily configured optical microstructures during the tuning process and they rapidly return to the original photonic crystal structures once the external driving forces are removed.<sup>[19,23]</sup>

Photonic crystals with optically bistable states, which complement currently available tunable photonic crystals, could provide a unique opportunity in realizing reconfigurable and rewritable optical devices.<sup>[32,33]</sup> For example, in sharp contrast with traditional subtractive microfabrication (e.g., photolithography followed by reactive ion etching),<sup>[34]</sup> functional optical microstructures can be patterned, erased, and rewritten on these optically bistable photonic crystals to accommodate different application needs.<sup>[33,35,36]</sup> This could dramatically reduce the complexity and fabrication cost of developing a large number of application-specific photonic crystal devices.<sup>[33]</sup> Shape memory polymers (SMPs), which can memorize and recover their permanent shapes in response to various external stimuli (e.g., heat, solvent, light, electrical and magnetic fields),<sup>[37–47]</sup> may hold the key to reconfigurable photonic crystals with bistable or even multistable states. They have also been widely used in a spectrum of applications ranging from smart surgical stents and sutures to aerospace morphing structures.<sup>[48,49]</sup> Shape memory (SM) for thermoresponsive SMPs is usually achieved in three steps including programming, storage, and recovery.<sup>[39,40]</sup> In SM programming, an SMP sample in its permanent shape is heated above a specific transition temperature ( $T_m$ ), such as the polymer glass transition temperature ( $T_g$ ), and then deformed to a temporary shape. After cooling below  $T_m$ , the sample can store the “frozen” temporary shape at ambient conditions for a long period of time. Finally, the memorized permanent shape can be recovered when the sample is reheated above  $T_m$ , and entropy elasticity of SMPs accounts for the shape restoration.<sup>[39,40]</sup>

Although the mechanically stable permanent and temporary shapes of SMPs could enable reconfigurable photonic crystals with optically bistable states, smart SMPs have rarely been used in previous photonic crystal studies.<sup>[50–54]</sup> Programmable and shape-memorizing microoptical devices, such as 2D microlens and micropism arrays, diffraction gratings, and holograms, have been demonstrated by using a semicrystalline SM elastomer—crosslinked poly(ethylene-co-vinyl acetate).<sup>[51,55]</sup> Similar thermoresponsive shape-memory 2D photonic crystals consisting of periodic microbowls (templated from 870 nm polystyrene microspheres) in a polydiolcitrate-based elastomer have recently been demonstrated as active diffractive elements for

Y. Fang, S.-Y. Leo, B. C. Wang, Prof. P. Jiang  
Department of Chemical Engineering  
University of Florida

Gainesville, FL 32611, USA  
E-mail: pjiang@che.ufl.edu

Y. L. Ni, Prof. C. Taylor  
Department of Mechanical and  
Aerospace Engineering  
University of Florida  
Gainesville, FL 32611, USA

Dr. L. Yu  
Department of Materials Science  
and Engineering  
University of Florida  
Gainesville, FL 32611, USA

P. X. Qi  
Department of Chemistry  
University of Florida  
Gainesville, FL 32611, USA

Dr. V. Basile  
ITIA-CNR  
Industrial Technologies and Automation Institute  
National Council of Research  
Via Bassini 15, 20133 Milano, Italy

DOI: 10.1002/adom.201500277



various optical applications.<sup>[50]</sup> 3D ordered elastomeric polymer opal films, which exhibit tunable and reversible PBGs triggered by light, heat, and mechanical strains, have been assembled by using specifically engineered core-interlayer-shell (CIS) polymer microspheres.<sup>[52,53,56]</sup> Unfortunately, the SMP-enabled tunable photonic crystals in these previous studies suffer from either low-PBG (indeed optical stop band) amplitudes caused by the 2D nature of the surface gratings or limited material selection. Here we report a generalized templating approach for fabricating thermoresponsive 3D macroporous SMP photonic crystals with optically bistable states. The technology can be easily applied to nearly all functional SMPs, provided they can survive the template removal process, such as a brief hydrofluoric acid wash for removing the templating silica colloidal crystals. In addition, the templated 3D macroporous SMP photonic crystals with high crystalline qualities exhibit much stronger diffractive effects than 2D surface gratings.<sup>[57]</sup> Moreover, the heat-triggered transition between a disordered temporary state and a 3D ordered permanent state leads to an easily perceived color change and a significant difference in their optical responses. Furthermore, the 3D photonic crystal structure enables a simple and sensitive optical technology for quantitatively characterize the intriguing SM effects at nanoscale.<sup>[58]</sup>

The thermoresponsive macroporous SMP photonic crystal membranes with 3D ordered macropores were prepared by templating fabrication using self-assembled silica colloidal crystals as structural templates.<sup>[57,59]</sup> The convective self-assembly technology was utilized in organizing monodispersed silica microspheres with 300 nm diameter into highly ordered colloidal single crystals.<sup>[60]</sup> The crystal thickness was controlled to  $\approx 5 \mu\text{m}$  by adjusting the particle volume fraction of the silica microspheres/ethanol suspension to  $\approx 1.0\%$ . Through capillary interactions, the interstitial air in between the close-packed silica microspheres was replaced by a commercial oligomer mixture (CN745A70, Sartomer, viscosity 2200 cps at 60 °C, refractive index 1.4795) consisting of trifunctional acrylated urethane and tripropylene glycol diacrylate (TPGDA). The oligomer mixture was then photopolymerized by exposing to UV radiation. We termed the resulting polyester/polyether copolymer as PU-co-TPGDA in this paper. The templating silica microspheres were finally removed by wet-etching in a 1 vol% hydrofluoric acid aqueous solution. The final self-standing macroporous SMP membranes are rigid and show brilliant diffractive colors that depend on the size of the macropores and the viewing angle.<sup>[57,61]</sup> In this paper, we used the commercial PU-co-TPGDA copolymer as a model thermoresponsive SMP, though the technology can be easily applied to many other types of SMPs.

The glass transition temperature of the PU-co-TPGDA copolymer, which is a critical parameter in heat-induced SM programming and recovery processes, was evaluated by differential scanning calorimetry (DSC). The typical DSC plot of a macroporous copolymer membrane in Figure 1a shows a single  $T_g$  of  $\approx 85.6$  °C, indicating the crosslinked copolymer is a homogeneous mixture of the two components. In addition, no apparent crystallization dips show up in the DSC plot for temperature from 0 to 200 °C (see the complete DSC plot with both heating and cooling cycles in Figure S1 in the Supporting Information), confirming that the copolymer is amorphous in

this temperature range.<sup>[62]</sup> The Young's modulus of the templated macroporous copolymer membrane was characterized by *in situ* nanoindentation tests. Figure 1b compares the average moduli of three membranes with 300 nm macropores indented by applying 100 mN force. More than 30 points on each sample

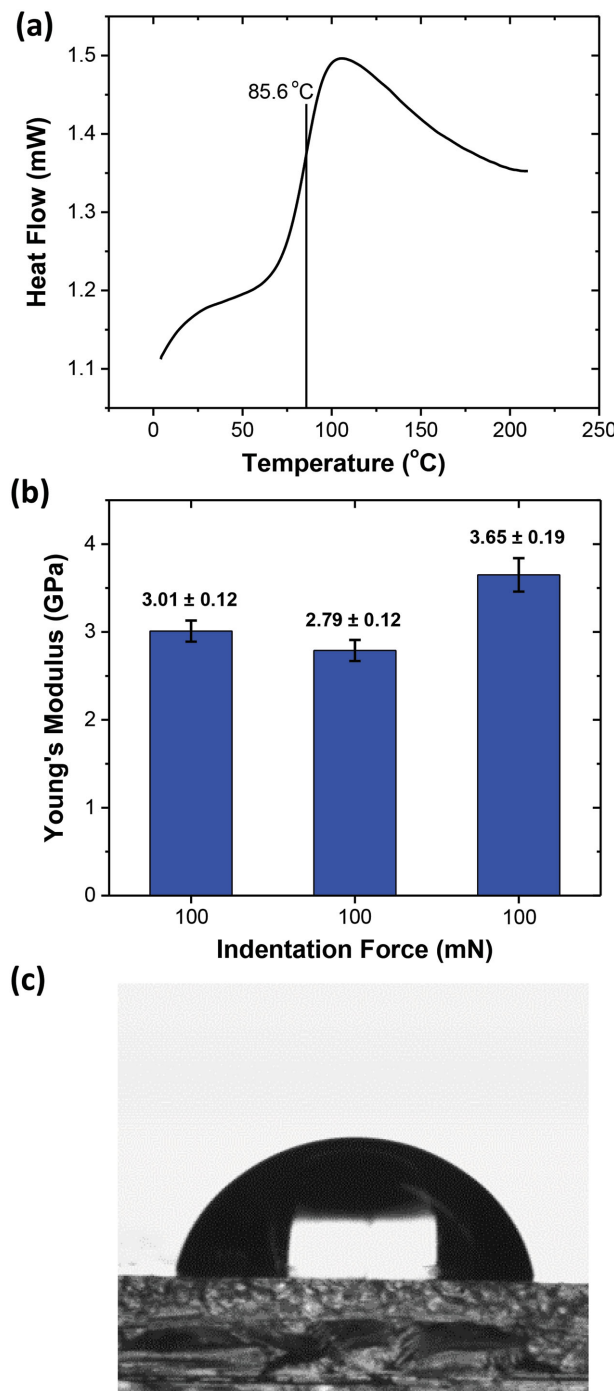


**Figure 1.** a) Typical DSC plot of PU-co-TPGDA copolymer. b) Young's modulus of three macroporous PU-co-TPGDA copolymer membranes indented with the same force (100 mN). c) Water drop profile on a freshly prepared macroporous PU-co-TPGDA membrane with 300 nm macropores.

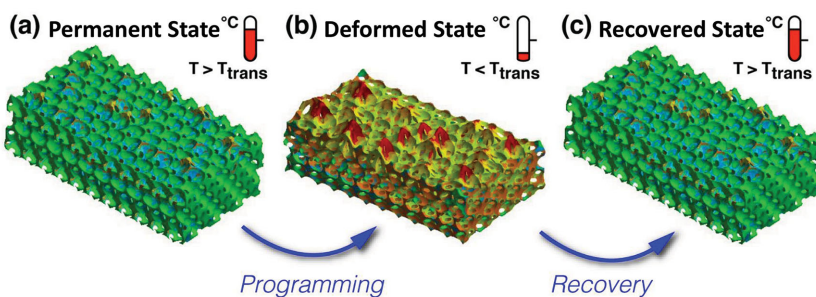


**Figure 2.** Schematic illustration showing the heat-induced programming and recovery steps of a thermoresponsive macroporous SMP photonic crystal membrane. a) Permanent state with 3D ordered macropores. b) Deformed state with collapsed macropores. c) Recovered state with reopened macropores. These images were constructed using a finite element method (FEM) model under an ANSYS environment. The colors were manipulated in order to give a better idea of the deformed and the undeformed shapes.

were measured to obtain the average modulus and its standard deviation. All three macroporous samples possess Young's modulus of  $\approx 3$  GPa, which is higher than the modulus measured by conventional tensile tests ( $\approx 1.4$  GPa with tensile strength of  $\approx 110$  MPa and yielding strain of  $\approx 0.08$ , provided by the vendor). The typical water drop profile in Figure 1c shows that the macroporous PU-co-TPGDA copolymer is nearly hydrophobic with an apparent water contact angle (CA) of  $80.7^\circ \pm 2.4^\circ$ .

The high  $T_g$  and mechanical strength, as well as the hydrophobic properties, make the PU-co-TPGDA copolymer a good candidate for making reconfigurable/rewritable photonic crystals with high durability and environmental stability. The schematic illustrations in Figure 2 show the microstructural transitions of a macroporous PU-co-TPGDA photonic crystal membrane during heat-induced SM programming and recovery processes. In programming, the original, 3D highly ordered macropores (permanent state) are deformed into disordered arrays when the copolymer sample is heated above its  $T_g$ , while a sufficient pressure is simultaneously applied on the softened copolymer. The deformed sample is then cooled below  $T_g$  to fix the temporary shape (disordered array) which can be stored at room temperature for a long period of time. SM recovery to the permanent, 3D ordered structure occurs when the deformed sample is reheated to above  $T_g$ . Similar to conventional thermoresponsive SMPs, entropy elasticity is believed to be the major reason for the heat-triggered macropore recovery.<sup>[39]</sup>

The photographs and the corresponding cross-sectional scanning electron microscope (SEM) images in Figure 3 show the color and microstructure changes of a macroporous PU-co-TPGDA membrane with 300 nm macropores transited from the permanent state (Figure 3a,b) to the deformed state (Figure 3c,d), and then to the recovered state (Figure 3e,f). The original macroporous copolymer film exhibits a shining greenish color (Figure 3a) which is caused by Bragg diffraction of visible light from the 3D highly ordered macroporous photonic crystal (see the cross-sectional SEM image in Figure 3b).<sup>[57]</sup> The diffractive color disappeared (Figure 3c) when the sample was heated to  $90^\circ\text{C}$ , while a clamp force of 200 lb was applied through a rectangle-shaped glass piece ( $\approx 1.5 \times 3.7$  cm) using a manual hydraulic press. After cooling down the sample to room temperature and releasing the

clamp force, the deformed region became nearly transparent with an average optical transmittance (between 400 and 800 nm) of  $\approx 86\%$ , which was slightly lower than that of a plain PU-co-TPGDA film ( $\approx 90\%$ ). The loss of periodicity of the original photonic crystal structure and the deformation of the spherical macropores, which can be clearly seen from the cross-sectional SEM image in Figure 3d, is attributed to the discoloration of the membrane. In addition, the average thickness of the macroporous layer significantly reduced from  $\approx 5.2$  to  $\approx 3.2$   $\mu\text{m}$  in the above heat-induced programming process. This abrupt change in film thickness led to the clear edges between the colorful and the transparent regions in Figure 3c.

The retention of the greenish color around the upper right corner of the rectangular box was caused by a defect in the stainless steel chamber of the hydraulic press which affected the even distribution of pressure applied on the macroporous sample.

The disordered array of collapsed macropores can be recovered back to the permanent photonic crystal structure by reheating the deformed sample above  $T_g$  of the PU-co-TPGDA copolymer. Figure 3e shows the same sample as Figure 3c after heating the membrane in an oven at  $90^\circ\text{C}$  for 2 min. The recovery of the vivid greenish color of the deformed rectangular region is clearly evident. The cross-sectional SEM image in Figure 3f confirms the restoration of the ordered photonic crystal structure after the above thermal treatment. However, our extensive SEM characterization indicated that the heat-triggered macropore recovery is not fully complete (i.e., the strain recovery rate is not 100%). The average thickness of the recovered macroporous layer in Figure 3f is  $\approx 4.9$   $\mu\text{m}$ , which is about 94% of the thickness of the original macroporous photonic crystal. Additionally, by comparing the SEM images in Figure 3b,f, it is apparent that the surface of the restored macroporous layer is not as smooth as the original sample, further indicating the incomplete macropore recovery. To quantitatively characterize the surface microstructures of the macroporous photonic crystals in the heat-induced SM programming and recovery processes, we conducted extensive atomic force microscopy (AFM) imaging. Figure 4 presents AFM topographic images and the corresponding height profiles scanned across the dashed lines for the same macroporous samples as shown in Figure 3. The surface of the original photonic crystal is smooth and the templated macropores are highly ordered (see Figure 4a,b). By contrast, the same sample in the deformed state (Figure 4c,d) has a much rougher surface and the ordered macroporous structure is entirely lost, similar to the cross-sectional SEM image as shown in Figure 3d. The partial recovery of the original smooth surface and the long-range ordering of the macropores are apparently shown by the recovered sample (Figure 4e,f). The significant changes in surface roughness can be quantitatively characterized by the root mean square (RMS) roughness,  $R_q$ , using AFM topographic images. The average  $R_q$  is  $8.8 \pm 0.7$  nm,  $47.9 \pm 16.2$  nm, and  $14.0 \pm 1.9$  nm, corresponding to the above three samples with the

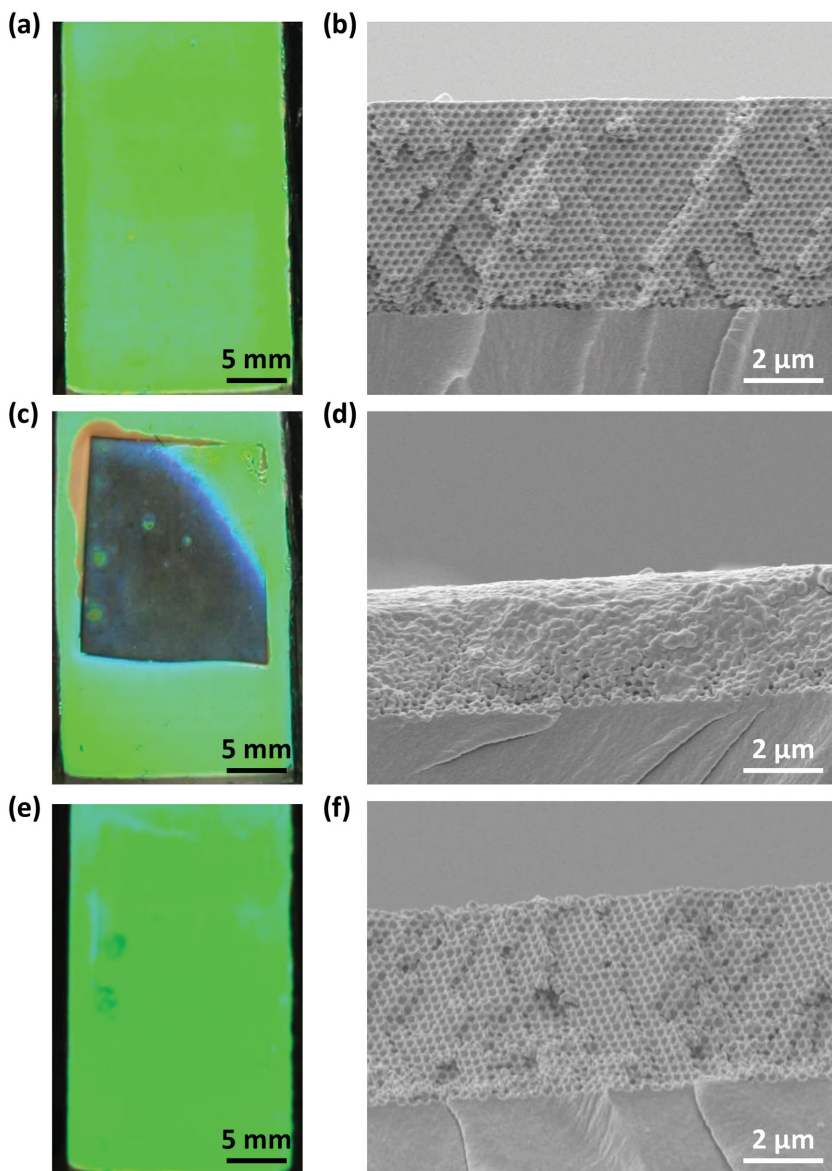


**Figure 3.** Photographs and SEM images showing the apparent changes in reflective colors and microstructures during heat-induced programming and recovery steps of a macroporous PU-co-TPGDA copolymer membrane with 300 nm macropores. a,b) Permanent state with 3D ordered macropores. c,d) Deformed state with collapsed macropores. e,f) Thermally recovered state with reopened macropores.

permanent, deformed, and recovered states, respectively. The surface of the deformed sample is substantially rougher than the original and the recovered samples.

The microstructural transition associated with the heat-induced SM programming and recovery processes, which induces easily perceived color changes, can be quantitatively characterized by normal-incidence optical reflection measurements. **Figure 5** compares the reflection spectra obtained from the same macroporous SMP sample with 300 nm macropores in the permanent state (red curve), deformed state (black curve), and recovered state (blue curve). The original macroporous photonic crystal with 3D highly ordered macropores (see Figure 3b) exhibits a strong PBG peak at  $\approx 539$  nm with well-defined

Fabry–Perot fringes. The PBG peak position agrees with the calculation using the Bragg diffraction equation:

$$\lambda_{\max} = 2 \times n_{\text{eff}} \times d \times \sin \theta \quad (1)$$

where  $n_{\text{eff}}$  is the effective refractive index of the macroporous photonic crystal ( $\approx 1.12$  by assuming the refractive index of the SMP copolymer is 1.47 and the volume fraction of the copolymer and air is 0.26 and 0.74, respectively),  $d$  is the interplane distance ( $300 \times \sqrt{2/3}$  nm), and  $\theta = 90^\circ$  for normal incidence. Moreover, the experimental reflection spectrum of the macroporous sample in the permanent state matches well with the theoretical spectrum (green curve) simulated using a scalar wave approximation (SWA) model,<sup>[63]</sup> which assumes a perfect face-centered cubic (f.c.c.) structure with the (111) crystalline planes parallel to the sample surface.

In sharp contrast with the distinct PBG peak displayed by the original macroporous SMP photonic crystal, the deformed sample with disordered macropores (see Figure 3d) shows no apparent PBG peaks in the normal-incidence reflection spectrum. This complete discoloration represents a major difference between traditional tunable photonic crystals<sup>[10,18–28,64]</sup> and the new SMP-enabled photonic crystals. For traditional tunable photonic crystals, the PBG peaks shift to different locations depending on the changes in the lattice spacing and/or effective refractive index. The wavelength shift is usually limited and the PBG peak returns to the original position once the external stress is released. This means that the temporarily deformed photonic crystal structures cannot be memorized. By contrast, the new SMP-enabled photonic crystals exhibit two optically stable states corresponding to the permanent (ordered) and the temporary (disordered) states of the macropores. This manifest order-disorder transition leads to

the easily perceived color change and a large  $\Delta\lambda_{\max}$  (indeed it equals to  $\lambda_{\max}$  of the original photonic crystal as no PBG exists in the deformed state). When the deformed macropores recovered back to the 3D ordered photonic crystal structure by reheating the sample above  $T_g$  of the copolymer, the PBG peak and the Fabry–Perot fringes reappeared in the reflection spectrum. However, similar to the aforementioned SEM and AFM analysis, the amplitude of the PBG peak is only partially recovered. In addition, the peak position slightly blueshifts to  $\approx 530$  nm, agreeing with the small decrease in the macroporous layer thickness as observed by SEM imaging. Moreover, the spectrum obtained from the second recovered state (i.e., the macroporous SMP membrane was mechanically deformed and

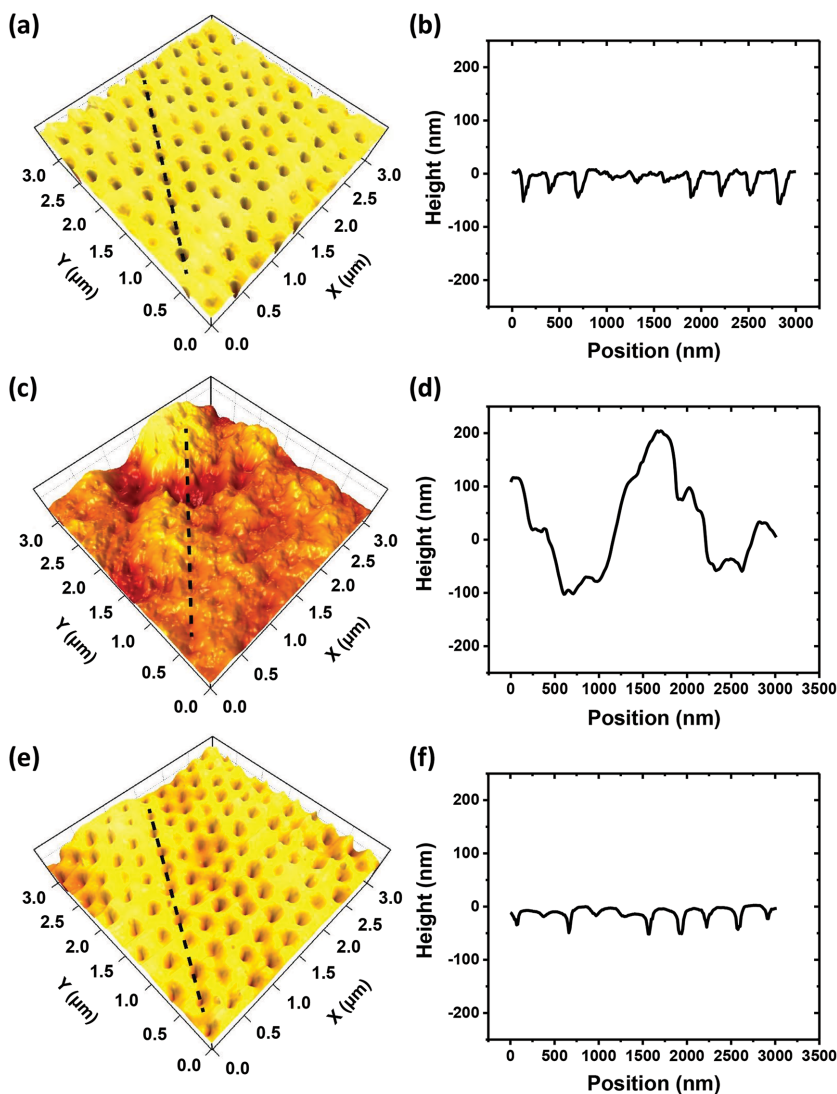


**Figure 4.** AFM images and the corresponding height profiles (across the dashed lines) showing the changes in surface microstructures during heat-induced programming and recovery steps of a macroporous PU-co-TPGDA copolymer membrane with 300 nm macropores. **a,b)** Permanent state with ordered macropores. **c,d)** Deformed state with collapsed macropores. **e,f)** Thermally recovered state with reopened macropores.

then thermally recovered again) matches reasonably well with the spectrum of the first recovered state, indicating good repeatability of the heat-triggered SM recovery process.

Above, we have shown that optical reflection measurements provide a straightforward and sensitive methodology in characterizing microscopic structural changes of macroporous SMP photonic crystals associated with heat-induced SM programming and recovery. This simple optical technology also enables *in situ* characterization of the SM recovery dynamics of the thermoresponsive PU-co-TPGDA copolymer. Figure 6a shows the stacked optical reflection spectra obtained from a macroporous SMP sample which was placed on a hot plate preset at  $90 \pm 1$  °C. The optical spectrometer was set to automatically collect a whole reflection spectrum every second. The color-coded reflection amplitude gradually increases with

longer heating duration and it reaches a plateau after  $\approx 200$  s. This can be easily seen from the 2D representation of the time-resolved reflection spectra in Figure 6b. Considering the slow heat conduction through a thick, solid copolymer backing layer ( $\approx 1700$   $\mu\text{m}$  thick) to the top macroporous layer (only  $\approx 5$   $\mu\text{m}$  thick), as well as the inevitable heat dissipation into the surrounding environment (at room temperature), it will take a while for the top SMP photonic crystal layer to be above its  $T_g$ . Therefore, we believe that the real SM recovery response speed at 90 °C should be much less than 200 s. Indeed, the SM recovery speed is a sensitive function of the reheating temperature.<sup>[65]</sup> Our experiment showed that a deformed SMP membrane recovered its vivid diffractive color within 3 s when the macroporous layer was directly heated by a heat gun and the temperature nearby the SMP membrane was  $\approx 100$  °C measured by a digital thermometer.

The thermoresponsive SMP photonic crystals can be reused for at least several tens of times without apparent degradation in their optical performance. Figure 7 shows the absolute reflection amplitudes at 530 nm and the corresponding photographs of a macroporous PU-co-TPGDA copolymer membrane (O1) being cyclically deformed (D1, D2, D3, D4, D5) and recovered (R1, R2, R3, R4, R5). The deformed and the recovered regions exhibit similar colors and absolute reflection amplitudes, indicating the high reproducibility of the heat-induced SM programming and recovery processes. This reversibility is critically important for developing reconfigurable/rewritable photonic devices.<sup>[32,33]</sup>

In conclusion, we have developed a universal templating nanofabrication technology for making 3D macroporous SMP photonic crystals with optically bistable states. The heat-induced transition between an ordered permanent state and a disordered temporary state leads to tremendous changes in the appearance and the diffractive properties of the photonic crystals. The high reproducibility in optical responses during multiple SM programming-recovery cycles, high  $T_g$  and mechanical strength, and hydrophobicity of the model PU-co-TPGDA copolymer demonstrate its merits in making reconfigurable/rewritable photonic crystal devices. Although the smallest size of features that can be patterned and then thermally recovered is  $\approx 300$   $\mu\text{m}$ , our preliminary results showed that much finer photonic crystal microfeatures with  $<30$   $\mu\text{m}$  resolution could be reversibly fabricated by using a new PU-co-TPGDA copolymer with a different composition and a lower  $T_g$ . Importantly, the thin macroporous photonic crystal structure enables a simple, quantitative, and sensitive optical technology for investigating the intriguing nanoscopic

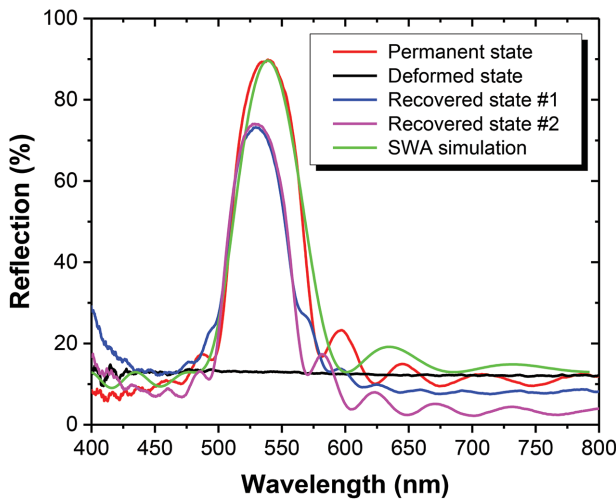


**Figure 5.** Normal-incidence optical reflection spectra showing the permanent, deformed, and two thermally recovered states of a macroporous PU-co-TPGDA copolymer membrane with 300 nm macropores. The simulated spectrum using an SWA model is also shown to compare with the experimental measurements.

SM effects (e.g., recovery dynamics). In addition to reconfigurable nanooptical devices, the thermoresponsive macroporous SMP membranes with reversible open or closed macropores could find many other applications, such as hydrophobic coatings with programmable wettability, smart membranes for

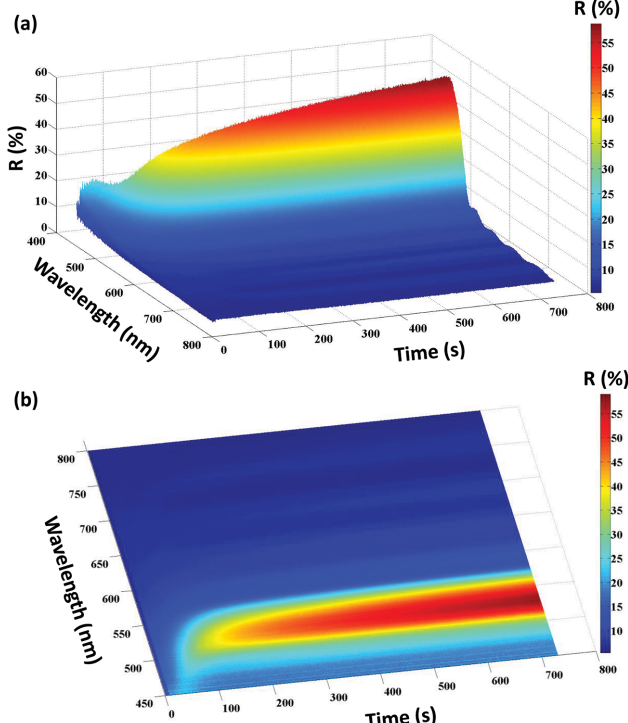


**Figure 6.** Time-resolved, color-coded normal-incidence optical reflection spectra during thermally induced recovery of a macroporous PU-co-TPGDA copolymer membrane with collapsed 300 nm macropores. a) 3D plot. b) 2D plot.

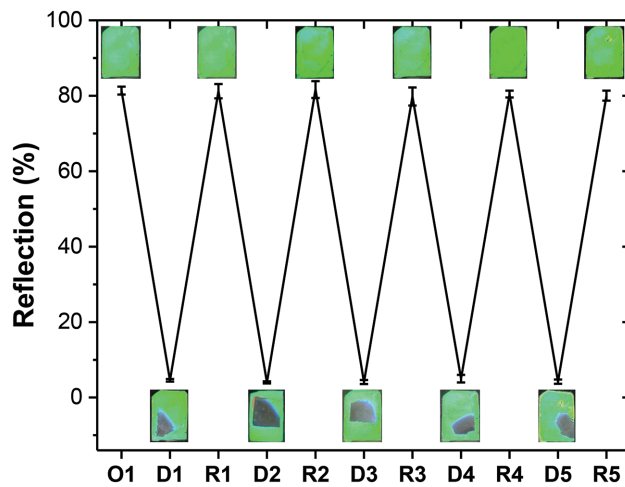


**Figure 7.** Reflection amplitudes at 530 nm wavelength and the corresponding photographs of a macroporous PU-co-TPGDA copolymer membrane with 300 nm macropores cyclically deformed (D1, D2, D3, D4, D5) and recovered (R1, R2, R3, R4, R5). O1 indicates the original sample.

size-exclusive filtration, and light-regulating coatings for energy-efficient buildings.<sup>[66–68]</sup>

## Experimental Section

**Templating Fabrication of Thermoresponsive Macroporous SMP Photonic Crystal Membranes:** Monodispersed silica microspheres with 300 nm diameter were synthesized by the standard Stöber method.<sup>[69]</sup> The resulting silica particles with diameter standard deviation less than 5% were purified in 200-proof ethanol by multiple centrifugation and redispersion cycles (at least five times). The purified silica microspheres were then self-assembled on a glass microslide by the convective self-assembly technology to form close-packed multilayer colloidal crystals.<sup>[60]</sup> The crystal thickness was controlled to  $\approx$ 5  $\mu$ m (or  $\approx$ 20 colloidal monolayers) by adjusting the particle volume fraction of the silica microspheres–ethanol suspension. A double-sided adhesive tape ( $\approx$ 1.7 mm thick) was used as a spacer to separate the microslide with the assembled colloidal crystal on its surface and a bare glass microslide. The viscous oligomer mixture (CN745A70, Sartomer) consisting of trifunctional acrylated urethane and TPGDA was preheated at 90 °C for 5 min. Darocur 1173 (2-hydroxy-2-methyl-1-phenyl-1-propanone, BASF, 0.8 wt%) was added as the photoinitiator. The oligomer mixture was injected in the above microslide sandwich cell. The replacement of air in between silica microspheres with the index-matching oligomer mixture made the cell transparent. The sample was transferred to a pulsed UV curing system (RC 742, Xenon) and the oligomer mixture was rapidly polymerized by exposure to UV radiation for 4 s. The polymerized film was immersed in a 1 vol% hydrofluoric acid aqueous solution for 48 h and then rinsed with deionized water. After blow-drying with compressed air, the final self-standing macroporous PU-co-TPGDA copolymer membrane showed striking iridescent colors.

**Heat-Induced SM Programming and Recovery:** The templated macroporous SMP copolymer membrane was placed in between a precleaned glass substrate and a smaller glass piece. The sample was then held by two stainless steel plates and a clamp force of 200 lb was applied using a manual hydraulic press (Carver Model C). The temperature of the system rapidly increased from room temperature to  $\approx$ 90 °C and stayed at this temperature for 3 min. The sample then cooled down to room temperature. After releasing the clamp force, the pressed region became nearly transparent. The deformed sample

was finally placed in an oven preset at 90 °C for 2 min to recover the deformed macropores.

**Sample Characterization:** SEM imaging was carried out on an FEI Nova NanoSEM 430. A thin layer of gold was sputtered onto the samples prior to imaging. Amplitude-modulation atomic force microscopy (AM-AFM) was performed using an MFP-3D AFM (Asylum Research) with a Nanosensor PPP-NCHR probe (tip radius <10 nm). In situ nanoindentation tests were conducted using an MFP-3D NanoIndenter (Asylum Research) with a spherical sapphire indenter (tip radius ≈125 μm). Such configuration of the instrument has a force and displacement resolution less than 3 pN and 1 nm, respectively. Differential scanning calorimetric measurements were performed from 0 to 200 °C at a heating rate of 10 °C min<sup>-1</sup> using a TA Instruments DSC Q1000 and an empty pan as reference. The apparent water contact angle was measured using a goniometer (NRL C.A. Goniometer, Ramé-Hart Inc.) with autopipetting and imaging systems. Normal-incidence optical reflection spectra were taken using an Ocean Optics HR4000 high-resolution fiber optic vis–NIR spectrometer with a reflection probe (R600–7) and a tungsten halogen light source (LS-1). Absolute reflectivity was obtained as the ratio of the sample spectrum and a reference spectrum, which was the optical density obtained from an aluminum-sputtered (1000 nm thickness) silicon wafer.

**Scalar Wave Approximation Optical Modeling:** The scalar wave theory implemented for periodic dielectric structures was utilized in modeling the normal-incidence optical reflection spectra from templated macroporous SMP photonic crystals.<sup>[63]</sup> In this theory, Maxwell's equations are solved for a periodic dielectric assuming that one may neglect diffraction from all but one set of crystalline planes (e.g., (111) planes in this work). No adjustable parameters were used in SWA modeling, since the size of the macropores and the crystal thickness can be independently determined by SEM, and the refractive index of the copolymer is known.

## Supporting Information

Supporting Information is available from the Wiley Online Library or from the author.

## Acknowledgements

Acknowledgments were made to the US Defense Threat Reduction Agency (DTRA) under Contract No. HDTRA1-15-1-0022, US National Aeronautics and Space Administration (NASA) under Grant Award No. NNX14AB07G, US National Science Foundation (NSF) under Award No. CMMI-1300613, and Marie Curie IRSES Project 247614-NET4m.

Received: May 21, 2015

Revised: July 10, 2015

Published online:

- [1] J. D. Joannopoulos, R. D. Meade, J. N. Winn, *Photonic Crystals: Molding the Flow of Light*, Princeton University Press, Princeton, NJ, USA 1995.
- [2] C. Lopez, *Adv. Mater.* **2003**, *15*, 1679.
- [3] Y. Yin, J. Ge, *J. Mater. Chem. C* **2013**, *1*, 6001.
- [4] J. H. Moon, S. Yang, *Chem. Rev.* **2010**, *110*, 547.
- [5] J. F. Galisteo-Lopez, M. Ibáñez, R. Sapienza, L. S. Froufe-Perez, A. Blanco, C. Lopez, *Adv. Mater.* **2011**, *23*, 30.
- [6] S. H. Kim, W. C. Jeong, S. M. Yang, *Chem. Mater.* **2009**, *21*, 4993.
- [7] A. C. Arsenault, D. P. Puzzo, I. Manners, G. A. Ozin, *Nat. Photonics* **2007**, *1*, 468.
- [8] N. L. Smith, Z. Hong, S. A. Asher, *Analyst* **2014**, *139*, 6379.

- [9] J. H. Holtz, S. A. Asher, *Nature* **1997**, *389*, 829.
- [10] J. M. Weissman, H. B. Sunkara, A. S. Tse, S. A. Asher, *Science* **1996**, *274*, 959.
- [11] C. I. Aguirre, E. Reguera, A. Stein, *Adv. Funct. Mater.* **2010**, *20*, 2565.
- [12] D. Yang, S. Ye, J. Ge, *Adv. Funct. Mater.* **2014**, *24*, 3197.
- [13] M. G. Han, C. G. Shin, S.-J. Jeon, H. Shim, C.-J. Heo, H. Jin, J. W. Kim, S. Lee, *Adv. Mater.* **2012**, *24*, 6438.
- [14] I. B. Burgess, M. Loncar, J. Aizenberg, *J. Mater. Chem. C* **2013**, *1*, 6075.
- [15] I. B. Burgess, N. Koay, K. P. Raymond, M. Kolle, M. Loncar, J. Aizenberg, *ACS Nano* **2012**, *6*, 1427.
- [16] Y. Kang, J. J. Walish, T. Gorishnyy, E. L. Thomas, *Nat. Mater.* **2007**, *6*, 957.
- [17] R. A. Potyrailo, H. Ghiradella, A. Vertiatchikh, K. Dovidenko, J. R. Cournoyer, E. Olson, *Nat. Photonics* **2007**, *1*, 123.
- [18] E. P. Chan, J. J. Walish, A. M. Urbas, E. L. Thomas, *Adv. Mater.* **2013**, *25*, 3934.
- [19] A. C. Arsenault, T. J. Clark, G. Von Freymann, L. Cademartiri, R. Sapienza, J. Bertolotti, E. Vekris, S. Wong, V. Kitaev, I. Manners, R. Z. Wang, S. John, D. Wiersma, G. A. Ozin, *Nat. Mater.* **2006**, *5*, 179.
- [20] Y. Yue, T. Kurokawa, M. A. Haque, T. Nakajima, T. Nonoyama, X. Li, I. Kajiwara, J. P. Gong, *Nat. Commun.* **2014**, *5*, 4659.
- [21] S. Valkama, H. Kosonen, J. Ruokolainen, T. Haatainen, M. Torkkeli, R. Serimaa, G. Ten Brinke, O. Ikkala, *Nat. Mater.* **2004**, *3*, 872.
- [22] J. Q. Xia, Y. R. Ying, S. H. Foulger, *Adv. Mater.* **2005**, *17*, 2463.
- [23] J. Ge, J. Goebel, L. He, Z. Lu, Y. Yin, *Adv. Mater.* **2009**, *21*, 4259.
- [24] Y. Takeoka, M. Watanabe, *Langmuir* **2002**, *18*, 5977.
- [25] J. P. Ge, Y. D. Yin, *J. Mater. Chem.* **2008**, *18*, 5041.
- [26] S. Ye, Q. Fu, J. Ge, *Adv. Funct. Mater.* **2014**, *24*, 6430.
- [27] H. Fudouzi, Y. N. Xia, *Langmuir* **2003**, *19*, 9653.
- [28] D. Scheid, C. Lederle, S. Vowinkel, C. G. Schaefer, B. Stuehn, M. Gallei, *J. Mater. Chem. C* **2014**, *2*, 2583.
- [29] J. P. Ge, L. He, J. Goebel, Y. D. Yin, *J. Am. Chem. Soc.* **2009**, *131*, 3484.
- [30] H. Hu, C. Chen, Q. Chen, *J. Mater. Chem. C* **2013**, *1*, 6013.
- [31] Z. Pan, J. Ma, J. Yan, M. Zhou, J. Gao, *J. Mater. Chem.* **2012**, *22*, 2018.
- [32] W. S. Wang, N. Xie, L. He, Y. D. Yin, *Nat. Commun.* **2014**, *5*, 5459.
- [33] C. Grillet, C. Monat, C. L. Smith, M. W. Lee, S. Tormiljenovic-Hanic, C. Karnutsch, B. J. Eggleton, *Laser Photonics Rev.* **2010**, *4*, 192.
- [34] Y. A. Vlasov, X. Z. Bo, J. C. Sturm, D. J. Norris, *Nature* **2001**, *414*, 289.
- [35] D. Mao, X. Qiao, L. Dong, *J. Lightwave Technol.* **2013**, *31*, 1660.
- [36] T. Ding, Q. Zhao, S. K. Smoukov, J. J. Baumberg, *Adv. Opt. Mater.* **2014**, *2*, 1098.
- [37] M. Behl, M. Y. Razzaq, A. Lendlein, *Adv. Mater.* **2010**, *22*, 3388.
- [38] A. Lendlein, H. Y. Jiang, O. Junger, R. Langer, *Nature* **2005**, *434*, 879.
- [39] A. Lendlein, S. Kelch, *Angew. Chem., Int. Ed.* **2002**, *41*, 2034.
- [40] T. Xie, *Nature* **2010**, *464*, 267.
- [41] T. Xie, *Polymer* **2011**, *52*, 4985.
- [42] T. Xie, X. Xiao, J. Li, R. Wang, *Adv. Mater.* **2010**, *22*, 4390.
- [43] X. Gu, P. T. Mather, *RSC Adv.* **2013**, *3*, 15783.
- [44] P. T. Mather, X. Luo, I. A. Rousseau, *Annu. Rev. Mater. Res.* **2009**, *39*, 445.
- [45] W. M. Huang, B. Yang, Y. Q. Fu, *Polyurethane Shape Memory Polymers*, CRC Press, Boca Raton, FL, USA 2012.
- [46] H. Meng, J. Hu, *J. Intell. Mater. Syst. Struct.* **2010**, *21*, 859.
- [47] R. R. Kohlmeier, P. R. Buskohl, J. R. Deneault, M. F. Durstock, R. A. Vaia, J. Chen, *Adv. Mater.* **2014**, *26*, 8114.
- [48] G. Baer, T. Wilson, D. Maitland, D. Matthews, *J. Invest. Med.* **2006**, *54*, S162.
- [49] Y. Heo, H. A. Sodano, *Adv. Funct. Mater.* **2014**, *24*, 5261.
- [50] A. Espinha, M. Concepcion Serrano, A. Blanco, C. Lopez, *Adv. Opt. Mater.* **2014**, *2*, 516.

- [51] H. Xu, C. Yu, S. Wang, V. Malyarchuk, T. Xie, J. A. Rogers, *Adv. Funct. Mater.* **2013**, *23*, 3299.
- [52] C. G. Schaefer, M. Gallei, J. T. Zahn, J. Engelhardt, G. P. Hellmann, M. Rehahn, *Chem. Mater.* **2013**, *25*, 2309.
- [53] C. G. Schaefer, D. A. Smolin, G. P. Hellmann, M. Gallei, *Langmuir* **2013**, *29*, 11275.
- [54] J.-H. Jang, C. Y. Koh, K. Bertoldi, M. C. Boyce, E. L. Thomas, *Nano Lett.* **2009**, *9*, 2113.
- [55] Z. Wang, C. Hansen, Q. Ge, S. H. Maruf, D. U. Ahn, H. J. Qi, Y. Ding, *Adv. Mater.* **2011**, *23*, 3669.
- [56] C. G. Schaefer, C. Lederle, K. Zentel, B. Stuehn, M. Gallei, *Macromol. Rapid Commun.* **2014**, *35*, 1852.
- [57] P. Jiang, K. S. Hwang, D. M. Mittleman, J. F. Bertone, V. L. Colvin, *J. Am. Chem. Soc.* **1999**, *121*, 11630.
- [58] T. Altebaumer, B. Gotsmann, H. Pozidis, A. Knoll, U. Duerig, *Nano Lett.* **2008**, *8*, 4398.
- [59] O. D. Velev, S. Gupta, *Adv. Mater.* **2009**, *21*, 1897.
- [60] P. Jiang, J. F. Bertone, K. S. Hwang, V. L. Colvin, *Chem. Mater.* **1999**, *11*, 2132.
- [61] O. D. Velev, T. A. Jede, R. F. Lobo, A. M. Lenhoff, *Nature* **1997**, *389*, 447.
- [62] C. Schick, *Anal. Bioanal. Chem.* **2009**, *395*, 1589.
- [63] D. M. Mittleman, J. F. Bertone, P. Jiang, K. S. Hwang, V. L. Colvin, *J. Chem. Phys.* **1999**, *111*, 345.
- [64] A. Arsenault, S. B. Fournier-Bidoz, B. Hatton, H. Miguez, N. Tetrault, E. Vekris, S. Wong, S. M. Yang, V. Kitaev, G. A. Ozin, *J. Mater. Chem.* **2004**, *14*, 781.
- [65] J. Li, T. Xie, *Macromolecules* **2011**, *44*, 175.
- [66] H. T. Yang, P. Jiang, *Langmuir* **2010**, *26*, 12598.
- [67] X. Wang, S. M. Husson, X. Qian, S. R. Wickramasinghe, *J. Membr. Sci.* **2010**, *365*, 302.
- [68] D. Ge, E. Lee, L. Yang, Y. Cho, M. Li, D. S. Gianola, S. Yang, *Adv. Mater.* **2015**, *27*, 2489.
- [69] W. Stober, A. Fink, E. Bohn, *J. Colloid Interface Sci.* **1968**, *26*, 62.